Contemporary Mathematics
https://ojs.wiserpub.com/index.php/CM/

Research Article

Fractals Patterns as Mandelbrot Sets for a Complex Functions via Viscosity Approximation Iterative Method

Mohammad Sajid[1]*, Iqbal Ahmad[1], Mohammed D. Alharbi[2]

[1] Department of Mechanical Engineering, College of Engineering, Qassim University, Saudi Arabia
[2] Department of Electrical Engineering, College of Engineering, Qassim University, Saudi Arabia
E-mail: msajd@qu.edu.sa

Received: 25 September 2025; **Revised:** 28 October 2025; **Accepted:** 5 November 2025

Abstract: This article explores novel fractal patterns within Mandelbrot sets generated by a new class of complex functions of the forms $\Phi(z) = \vartheta z^p + \psi z + \log(\omega^\ell)$ and $\Psi(z) = \vartheta \cos(z^p) + \psi z + \log(\omega^\ell)$, where $p \geq 2$, ϑ, $\psi \in \mathbb{C}$, $\omega \in \mathbb{C}\backslash\{0\}$ and $\ell \in [1, \infty)$, where the traditional constant term is replaced with a logarithmic function. Utilizing a viscosity approximation-type iterative method, we develop escape criteria that enhance existing algorithms and enable the effective visualization of intricate Mandelbrot sets. Our findings reveal dynamic transformations in the shape and size of these fractals as key input parameters are varied. We believe that the insights gained from this study will inspire and motivate researchers and enthusiasts with a deep interest in fractal geometry.

Keywords: algorithms, iterative method, Mandelbrot sets, escape criteria, patterns

MSC: 28A80, 37F10, 39B12, 47H10

1. Introduction

While conventional geometry relies on simple forms like lines and circles, fractal geometry is essential for interpreting nature's true complexity. The Julia set, a fractal defined by Julia [1] through iterative functions like $z^2 + c$, was later visualized by Mandelbrot [2], who coined the term "fractal" and discovered the related Mandelbrot set. The real-world utility of Julia and Mandelbrot sets extends far beyond their mathematical beauty, modeling biological structures from nerve fibers to microbial growth, analyzing turbulent flows in physics, and enabling practical applications like fractal antennae in telecommunications and architectural models in radar systems (see [3–6]).

The advancement in generating and visualizing fractals, particularly Julia and Mandelbrot sets, is fundamentally rooted in the development of fixed-point iterative methods. The creation of these intricate structures hinges on a vital "escape criterion", a stopping rule that determines whether a point's orbit remains bounded or escapes to infinity. The development of iterative methods, beginning with fixed-point techniques and expanding to include Ishikawa, Noor, and Jungck-type iterations, has been fundamental in advancing their visualization and analysis (see [1, 2, 7–12]). Beyond their mathematical beauty, these sets possess significant real-world utility, modeling biological structures like nerve fibers, analyzing turbulent flows in physics, and enabling practical applications in telecommunications via fractal antennae (see [7, 8, 10, 13, 14]).

Copyright ©2026 Mohammad Sajid, et al.
DOI: https://doi.org/10.37256/cm.7220268722
This is an open-access article distributed under a CC BY license
(Creative Commons Attribution 4.0 International License)
https://creativecommons.org/licenses/by/4.0/

A recent study by Adhikari et al. [15] and Tanveer et al. [16] presented a substantial innovation in fractal theory through a modification of the classical n^{th} degree polynomial function. The authors substituted the constant parameter c with the sine expression $\sin(c^t)$ and the logarithmic expression $\log(c^t)$, where $t \in [1, \infty)$. They successfully established the necessary escape criteria for this new function under both Mann and Picard-Mann iterative schemes. The efficacy of this approach was confirmed through comprehensive graphical and numerical examples, which demonstrated that the parameter choices within the iterations directly govern the resulting fractal sets' distinct behavioral and structural properties.

Moreover, a generalized Halpern iteration or viscosity-type method introduced in [17] to generate Julia sets and biomorphs. This work was subsequently expanded through the integration of an s-convexity parameter to effectively generate Mandelbrot sets. Beyond their specific utility in fractal generation, these iterative procedures hold significant applications in fixed point theory, demonstrating considerable potential for creating a wider array of complex visual structures [14, 18].

This study extends the work of Tanveer et al. [16] for generating Mandelbrot sets. Specifically inspired by their innovative use of a logarithmic function by changing the constant term ω with $\log(\omega^\ell)$ (where $\omega \in \mathbb{C}\backslash\{0\}$ and $\ell \in [1, \infty)$), here applies the viscosity approximation iterative method with s-convexity to visualize Mandelbrot sets. A key contribution is the derivation of a escape criterion for two distinct classes of complex functions of the forms $\Phi(z) = \vartheta z^p + \psi z + \log(\omega^\ell)$, and $\Psi(z) = \vartheta \cos(z^p) + \psi z + \log(\omega^\ell)$, where $p \geq 2$, $p \in \mathbb{N}$, ϑ, $\psi \in \mathbb{C}$, $\omega \in \mathbb{C}\backslash\{0\}$ and $\ell \in [1, \infty)$. These advancements serve to broaden the existing theoretical framework while simultaneously yielding novel fractal patterns [19, 20], thereby highlighting the enduring significance of these constructs in computational, applied and pure mathematical works.

This article is structured into 5 sections to present this work. Section 2 introduces the required definitions and preliminary results that form the theoretical foundation of our work. We provide key results to give a general escape criterion for generating Mandelbrot sets by the viscosity approximation iterative method with s-convexity in Section 3. Section 4 describes computational algorithms and presents MATLAB-generated visualizations (R2024a, version 24.1.0.2537033, 64-bit) of fractals under different parameter configurations, accompanied by detailed discussions of the results. At the end, Section 5 provides concluding remarks that summarize our findings and suggest directions for future research.

2. Preliminaries

This section provides the essential definitions as well as preliminary results that form the basis of our work.

Definition 1 (Julia set [1]) For a complex function $\Psi : \mathbb{C} \to \mathbb{C}$ the filled Julia set F_Ψ is given as:

$$F_\Psi = \{z \in \mathbb{C} : \{|\Psi^k(z)|\}_{k=0}^{\infty} \text{ is bounded}\},$$

where Ψ^k denotes the k^{th} iterate of Ψ. The boundary of F_Ψ is called the Julia set.

Definition 2 (Mandelbrot set [11]) For a complex function $\Psi : \mathbb{C} \to \mathbb{C}$, the Mandelbrot set $\mathscr{M}$ is given as:

$$\mathscr{M} = \{\wp \in \mathbb{C} : F_\wp \text{ is connected}\},$$

where $F_\wp$ denotes the filled Julia set associated with $\Psi(z)$. Equivalently,

$$\mathscr{M} = \{\wp \in \mathbb{C} : |F_\wp^j(\zeta) \nrightarrow \infty \text{ as } n \to \infty\}.$$

where ζ is one of the critical points of $\Psi(z)$.

Definition 3 (s-convex combination [21]) For $z_1, z_2, z_3, \cdots, z_n \in \mathbb{C}$ and $s \in (0, 1]$, an s-convex combination is given as:

$$\tau_1^s z_1 + \tau_2^s z_2 + \tau_3^s z_3 + \cdots + \tau_n^s z_n.$$

where $\tau_k \geq 0$ and $\sum_{k=1}^{n} \tau_k = 1$, for $k \in \{1, 2, 3, \cdots, n\}$.

Consider the following complex functions $\Phi, \Psi : \mathbb{C} \to \mathbb{C}$ as:

$$\Phi(z) = \vartheta z^p + \psi z + \log(\omega^\ell). \tag{1}$$

$$\Psi(z) = \vartheta \cos(z^p) + \psi z + \log(\omega^\ell). \tag{2}$$

where $p \geq 2$, ϑ, $\psi \in \mathbb{C}$, $\omega \in \mathbb{C}\backslash\{0\}$ and $\ell \in [1, \infty)$. Further, let $A(z) = \hbar z + \wp$ be a complex contraction mapping with $\hbar, \wp \in \mathbb{C}$ and $|\hbar| < 1$.

In the article, let $\mu = \dfrac{\log(\omega^\ell)}{\omega}$. Consequently, we can express $\log(\omega^\ell) = \omega\mu$.

The viscosity approximation iterative method, first introduced by Maudafi [17] in the context of Hilbert spaces. It can be adapted to the complex plane. Beginning from an arbitrary initial point $z_0 \in \mathbb{C}$, it generates a sequence z_k defined by the iteration:

$$z_{k+1} = \lambda_k A(z_k) + (1 - \lambda_k)\Phi(z_k), \quad k \geq 0, \tag{3}$$

and

$$z_{k+1} = \lambda_k A(z_k) + (1 - \lambda_k)\Psi(z_k), \quad k \geq 0, \tag{4}$$

where $\lambda_k \in (0, 1)$, $\Phi, \Psi : \mathbb{C} \to \mathbb{C}$ and A is a contraction mapping.

For simplicity, we take $\lambda_k = \lambda$, $\lambda \in (0, 1)$ in this work. The literature features has several extensions of the convex combination, a notable one being the s-convex combination. This article introduces a novel viscosity approximation iterative method by integrating the classical concept of convex combinations with its s-convex extension. We establish the convergence of the resulting iterative orbit for a complex functions Φ and Ψ under the assumption that A is a contraction mapping on the complex plane.

$$z_{k+1} = \lambda^s A(z_k) + (1 - \lambda)^s \Phi(z_k), \quad k \geq 0, \tag{5}$$

and

$$z_{k+1} = \lambda^s A(z_k) + (1 - \lambda)^s \Psi(z_k), \quad k \geq 0, \tag{6}$$

where $z_0 \in \mathbb{C}$ uses as the initial point, Φ and Ψ are given in (1) and (2), $\lambda \in (0, 1)$, and $s \in (0, 1]$.

The core algorithms for generating these fractals rely on calculating escape criteria and utilizing the Maclaurin series expansion for cosine function.

$$|\cos(z^n)| = \left|\sum_{k=0}^{\infty} \frac{(-1)^k z^{2nk}}{(2k)!}\right| > |z^n| \left|\sum_{k=1}^{\infty} \frac{(-1)^k z^{n(2k-1)}}{(2k)!}\right| \geq |\tau||z^n|, \tag{7}$$

where $|\tau| \in (0, 1]$ except the values of $z \in \mathbb{C}$ for which $|\tau| = 0$ (see the details [9]).

3. Escape criteria for Mandelbrot sets

Escape criteria are fundamental to the creation of fractals, including Mandelbrot sets and their variants. Herein, we develop escape criteria for the considered complex functions define in (1) and (2) to investigate and contrast novel mutants of these foundational sets.

3.1 *Escape criteria for* $\Phi(z) = \vartheta z^p + \psi z + \log(\omega^\ell)$

In this subsection, we show escape criteria for a complex valued function $\Phi(z) = \vartheta z^p + \psi z + \log(\omega^\ell)$, where $p \geq 2$, ϑ, $\psi \in \mathbb{C}$, $\omega \in \mathbb{C}\backslash\{0\}$ and $\ell \in [1, \infty)$.

Theorem 1 Assume that $z_0 \in \mathbb{C}$ satisfies the condition

$$|z_0| \geq \max\{|\omega|, |\wp|\} > \left(\frac{1 + (1-\lambda s)(|\psi| + |\mu|) + \lambda s(1 + |\hbar|)}{(1-\lambda s)|\vartheta|}\right)^{\frac{1}{p-1}},$$

where $\lambda \in (0, 1)$ and $A(z) = \hbar z + \wp$ is a contraction mapping with $\hbar$, $\wp \in \mathbb{C}$ and $|\hbar| < 1$. Let the sequence $\{z_k\}$ be defined as

$$z_{k+1} = \lambda^s A(z_k) + (1-\lambda)^s \Phi(z_k). \tag{8}$$

Then, the sequence $\{z_k\}_{k=0}^{\infty}$ defined in (8) diverges to ∞, i.e., $|z_k| \to \infty$ as $k \to \infty$.

Proof. For $k = 0$, and s, $\lambda \in (0, 1]$, $\lambda^s \geq s\lambda$, and expanding $(1-\lambda)^s$ utilizing the binomial theorem up to the linear term in λ, we obtain

$$\begin{aligned}
|z_1| &= |\lambda^s A(z_0) + (1-\lambda)^s \Phi(z_0)| \\
&\geq |\lambda s(\hbar z + \wp) + (1-\lambda s)(\vartheta z_0^p + \psi z_0 + \log(\omega^\ell))| \\
&\geq |\lambda s(\hbar z + \wp) + (1-\lambda s)(\vartheta z_0^p + \psi z_0 + \mu\omega)| \\
&\geq |(1-\lambda s)(\vartheta z_0^p + \psi z_0 + \mu\omega| - |\lambda s(\hbar z_0 + \wp)|
\end{aligned}$$

$$\geq (1-\lambda s)|\vartheta z_0^p| - (1-\lambda s)|\psi z_0 + \mu\omega| - \lambda s|\hbar||z_0| - \lambda s|\wp|$$

$$\geq (1-\lambda s)|\vartheta||z_0^p| - (1-\lambda s)|\psi||z_0| - (1-\lambda s)|\mu||\omega|$$

$$- \lambda s|\hbar||z_0| - \lambda s|\wp|.$$

Our assumption $|z_0| \geq \max\{|\omega|, |\wp|\}$ yields that $-|\omega| \geq -|z_0|$ and $-|\wp| \geq -|z_0|$, we obtain

$$|z_1| \geq (1-\lambda s)|\vartheta||z_0^p| - (1-\lambda s)|\psi||z_0| - (1-\lambda s)|\mu||z_0| - \lambda s|\hbar||z_0| - \lambda s|z_0|$$

$$\geq (1-\lambda s)|\vartheta||z_0^p| - (1-\lambda s)(|\psi|+|\mu|)|z_0| - \lambda s(1+|\hbar|)|z_0|$$

$$= (1-\lambda s)|\vartheta||z_0^p| - \big((1-\lambda s)(|\psi|+|\mu|) + \lambda s(1+|\hbar|)\big)|z_0|$$

$$= |z_0|\bigg((1-\lambda s)|\vartheta||z_0^{p-1}| - \big((1-\lambda s)(|\psi|+|\mu|) + \lambda s(1+|\hbar|)\big)\bigg)$$

which implies that,

$$|z_1| \geq |z_0|\bigg((1-\lambda s)|\vartheta||z_0^{p-1}| - \big((1-\lambda s)(|\psi|+|\mu|) + \lambda s(1+|\hbar|)\big)\bigg). \tag{9}$$

Our assumptions that $|z_0| > \left(\dfrac{1+(1-\lambda s)(|\psi|+|\mu|)+\lambda s(1+|\hbar|)}{(1-\lambda s)|\vartheta|}\right)^{\frac{1}{p-1}}$, gives

$$\bigg((1-\lambda s)|\vartheta||z_0^{p-1}| - \big((1-\lambda s)(|\psi|+|\mu|) + \lambda s(1+|\hbar|)\big)\bigg) > 1.$$

Therefore, there exists a constant $\Gamma > 0$ such that

$$(1-\lambda s)|\vartheta||z_0^{p-1}| - \big((1-\lambda s)(|\psi|+|\mu|) + \lambda s(1+|\hbar|)\big) > \Gamma + 1 > 1. \tag{10}$$

Using (9) and (10), we have

$$|z_1| > (1+\Gamma)|z_0|.$$

In particular, $|z_1| > |z_0|$, and by iterating this process, we obtain $|z_k| > (1+\Gamma)^k|z_0|$. It follows that $|z_k| \to \infty$, as $k \to \infty$. □

We derive a refined escape criterion in Theorem 1 for the viscosity approximation iterative method (Eq. (8)).

Corollary 1 Let $|z_0| \geq \max\left\{|\omega|, |\wp|, \left(\frac{1+(1-\lambda s)(|\psi|+|\mu|)+\lambda s(1+|\hbar|)}{(1-\lambda s)|\vartheta|}\right)^{\frac{1}{p-1}}\right\}$. Then $|z_k| \to \infty$ as $k \to \infty$.

3.2 *Escape criteria for* $\Psi(z) = \vartheta\cos(z^p) + \psi z + \log(\omega^\ell)$

In this subsection, we discuss escape criteria for a function $\Psi(z) = \vartheta\cos(z^p) + \psi z + \log(\omega^\ell)$, where $p \geq 2$, ϑ, $\psi \in \mathbb{C}$, $\omega \in \mathbb{C}\backslash\{0\}$ and $\ell \in [1, \infty)$.

Theorem 2 Assume that $z_0 \in \mathbb{C}$ satisfies the condition

$$|z_0| \geq \max\{|\omega|, |\wp|\} > \left(\frac{1+(1-\lambda s)(|\psi|+|\mu|)+\lambda s(1+|\hbar|)}{(1-\lambda s)|\vartheta||\tau|}\right)^{\frac{1}{p-1}},$$

where $\lambda \in (0, 1)$ and $A(z) = \hbar z + \wp$ is a contraction mapping with $\hbar, \wp \in \mathbb{C}$ and $|\hbar| < 1$. Let the sequence $\{z_k\}$ be defined as

$$z_{k+1} = \lambda A(z_k) + (1-\lambda)\Psi(z_k). \tag{11}$$

Then, the sequence $\{z_k\}_{k=0}^{\infty}$ defined in (11) diverges to ∞, i.e., $|z_k| \to \infty$, as $k \to \infty$.

Proof. For $k = 0$, and by (7), s, $\lambda \in (0, 1]$, we get $\lambda^s \geq s\lambda$, and expanding $(1-\lambda)^s$ utilizing the binomial theorem up to the linear term in λ, we obtain

$$\begin{aligned}
|z_1| &= |\lambda^s A(z_0) + (1-\lambda)^s \Psi(z_0)| \\
&\geq |\lambda s(\hbar z + \wp) + (1-\lambda s)(\vartheta\cos(z_0^p) + \psi z_0 + \log(\omega^\ell))| \\
&\geq |\lambda s(\hbar z + \wp) + (1-\lambda s)(\vartheta\cos(z_0^p) + \psi z_0 + \mu\omega)| \\
&\geq |(1-\lambda s)(\vartheta\cos(z_0^p) + \psi z_0 + \mu\omega| - |\lambda s(\hbar z_0 + \wp)| \\
&\geq (1-\lambda s)|\vartheta||\cos(z_0^p)| - (1-\lambda s)|\psi z_0 + \mu\omega| - \lambda s|\hbar||z_0| - \lambda s|\wp| \\
&\geq (1-\lambda s)|\vartheta||\tau|z_0^p| - (1-\lambda s)|\psi||z_0| - (1-\lambda s)|\mu||\omega| - \lambda s|\hbar||z_0| - \lambda s|\wp|.
\end{aligned}$$

Our assumption $|z_0| \geq \max\{|\omega|, |\wp|\}$ yields that $-|\omega| \geq -|z_0|$ and $-|\wp| \geq -|z_0|$, we obtain

$$|z_1| \geq (1-\lambda s)|\vartheta||\tau||z_0^p| - (1-\lambda s)|\psi||z_0| - (1-\lambda s)|\mu||z_0| - \lambda s|\hbar||z_0| - \lambda s|z_0|$$

$$\geq (1-\lambda s)|\vartheta||\tau||z_0^p| - (1-\lambda s)(|\psi|+|\mu|)|z_0| - \lambda s(1+|\hbar|)|z_0|$$

$$= (1-\lambda s)|\vartheta||\tau||z_0^p| - \big((1-\lambda s)(|\psi|+|\mu|) + \lambda s(1+|\hbar|)\big)|z_0|$$

$$= |z_0|\Bigg((1-\lambda s)|\vartheta||\tau||z_0^{p-1}| - \big((1-\lambda s)(|\psi|+|\mu|) + \lambda s(1+|\hbar|)\big)\Bigg)$$

which implies that,

$$|z_1| \geq |z_0|\Bigg((1-\lambda s)|\vartheta||\tau||z_0^{p-1}| - \big((1-\lambda s)(|\psi|+|\mu|) + \lambda s(1+|\hbar|)\big)\Bigg). \tag{12}$$

Our assumptions that $|z_0| > \left(\dfrac{1+(1-\lambda s)(|\psi|+|\mu|)+\lambda s(1+|\hbar|)}{(1-\lambda s)|\vartheta||\tau|}\right)^{\frac{1}{p-1}}$, gives

$$\Bigg((1-\lambda s)|\vartheta||\tau||z_0^{p-1}| - \big((1-\lambda s)(|\psi|+|\mu|) + \lambda s(1+|\hbar|)\big)\Bigg) > 1.$$

Therefore, there exists a constant $\Gamma > 0$ such that

$$(1-\lambda s)|\vartheta||\tau||z_0^{p-1}| - \big((1-\lambda s)(|\psi|+|\mu|) + \lambda s(1+|\hbar|)\big) > \Gamma + 1 > 1. \tag{13}$$

Using (12) and (13), we have

$$|z_1| > (1+\Gamma)|z_0|.$$

In particular, $|z_1| > |z_0|$, and by iterating this process, we obtain $|z_k| > (1+\Gamma)^k|z_0|$. It follows that $|z_k| \to \infty$ as $k \to \infty$. □

We derive a refined escape criterion in Theorem 2 for the viscosity approximation iterative method (Eq. (9)).

Corollary 2 Let $|z_0| \geq \max\left\{|\omega|, |\wp|, \left(\dfrac{1+(1-\lambda s)(|\psi|+|\mu|)+\lambda s(1+|\hbar|)}{(1-\lambda s)|\vartheta||\tau|}\right)^{\frac{1}{p-1}}\right\}$. Then $|z_k| \to \infty$ as $k \to \infty$.

4. Graphical results

This section showcases graphical demonstration of Mandelbrot sets generated through the viscosity approximation iterative method (Eq. (8) and Eq. (11)) by varying input parameters and exponents. Utilizing escape time algorithms with the criteria obtained in Section 3, these intricate fractal structures were computationally implemented in MATLAB

(version R2024a, 24.1.0.2537033, 64-bit) using a color map (see, Figure 1) to visualize the examples. The resulting visualizations, produced by the procedures detailed in Algorithms 1 and 2, demonstrate the complex geometries arising from different parameter configurations. To ensure reproducibility and enable a thorough analysis, certain parameter values and computational settings are used for every figure.

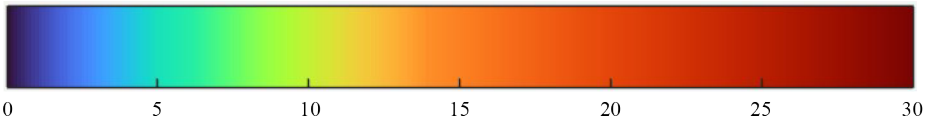


Figure 1. A color map is used in the examples

Algorithm 1 Generation of Mandelbrot sets for $\Phi(z) = \vartheta z^p + \psi z + \log(\omega^\ell)$

Input: $\Phi(z) = \vartheta z^p + \psi z + \log(\omega^\ell)$, where $p \geq 2$, $p \in \mathbb{N}$, ϑ, $\psi \in \mathbb{C}$, $\mu \in \mathbb{C}\backslash\{0\}$, $\ell \in [1, \infty)$. $A \subset \mathbb{C}$-area in which draw the set; K-maximal number of iterations; $\lambda \in (0, 1)$-parameter of the viscosity approximation iterative method; $A(z) = \hbar z + \wp$, where $\hbar$, $\wp \in \mathbb{C}$ and $|\hbar| < 1$; colourmap[0..C-1]-color with C colors.

Output: Mandelbrot set for area A

for $z_0 \in A$ **do**

$$\mu = \frac{\log(\omega^\ell)}{\omega} \text{ and } R = \left\{ |\omega|, |\wp|, \left(\frac{1 + (1-\lambda)(|\psi| + |\mu|) + \lambda(1 + |\hbar|)}{(1-\lambda)|\vartheta|} \right)^{\frac{1}{p-1}} \right\}$$

$k = 0$

$z_0 = \omega$

while $k \leq K$ **do**

$z_{k+1} = \lambda A(z_k) + (1-\lambda)\Phi(z_k)$

if $|z_{k+1}| \geq R$ then break end if

$k = k + 1$

$$j = \left\lfloor (C-1)\frac{k}{K} \right\rfloor$$

colour z_0 with colourmap $[j]$.

Algorithm 2 Generation of Mandelbrot sets for $\Psi(z) = \vartheta \cos(z^p) + \psi z + \log(\omega^\ell)$

Input: $\Psi(z) = \vartheta \cos(z^p) + \psi z + \log(\omega^\ell)$, where $p \geq 2$, $p \in \mathbb{N}$, ϑ, $\psi \in \mathbb{C}$, $\mu \in \mathbb{C}\backslash\{0\}$, $\ell \in [1, \infty)$. $A \subset \mathbb{C}$-area in which draw the set; K-maximal number of iterations; $\lambda \in (0, 1)$-parameter of the viscosity approximation iterative method; $A(z) = \hbar z + \wp$, where $\hbar$, $\wp \in \mathbb{C}$ and $|\hbar| < 1$; colourmap[0..C-1]-color with C colors.

Output: Mandelbrot set for area A

for $z_0 \in A$ **do**

$$\mu = \frac{\log(\omega^\ell)}{\omega} \text{ and } R = \left\{ |\omega|, |\wp|, \left(\frac{1 + (1-\lambda s)(|\psi| + |\mu|) + \lambda s(1 + |\hbar|)}{(1-\lambda s)|\vartheta||\tau|} \right)^{\frac{1}{p-1}} \right\}$$

$k = 0$

$z_0 = \omega$

while $k \leq K$ **do**

$z_{k+1} = \lambda A(z_k) + (1-\lambda)\Psi(z_k)$

if $|z_{k+1}| \geq R$ then break end if

$k = k + 1$

$$j = \left\lfloor (C-1)\frac{k}{K} \right\rfloor$$

colour z_0 with colourmap $[j]$.

4.1 *Mandelbrot sets for* $\Phi(z) = \vartheta z^p + \psi z + \log(\omega^\ell)$

For Ist example, we generate Mandelbrot sets by Algorithm 1 with the function $\Phi(z) = \vartheta z^p + \psi z + \log(\omega^\ell)$. The parameters are fixed as follows: $\lambda = 0.4$, and $s = 0.5$. To analyze the visual effects of parameter variation, we organize the output into four groups. Within each group, three of the parameters ϑ, ψ, ω, ℓ are held constant, and the fourth is varied. The execution times for generating images are also given in seconds.

(i) In Figure 2, fixed $\ell = 2$, $\psi = 0.8$, $\hbar = 0.1$, $\wp = 3$, while ϑ varies as: (a) 0.15, (b) 1.5, (c) 4.9, (d) 5.15, (e) $0.75i$, (f) $1.1 + 2.5i$.

(ii) In Figure 3, fixed $\ell = 3$, $\vartheta = 1.25$, $\hbar = 0.35$, $\wp = 5$, while ψ varies as: (a) 5.1, (b) $0.15i$, (c) $1.75 + 0.35i$.

(iii) In Figure 4, fixed $\ell = 5$, $\psi = 0.25$, $\vartheta = 0.5$, $\wp = 0.01$, while $\hbar$ varies as: (a) 0.5, (b) $0.18i$, (c) $0.4 + 0.8i$.

(iv) In Figure 5, fixed $\ell = 5$, $\psi = 0.5 + 0.25i$, $\vartheta = 0.2 + 0.15i$, $\hbar = 0.1 + 0.28i$, while $\wp$ varies as: (a) 0.3, (b) $3i$, (c) $0.08 + 0.03i$.

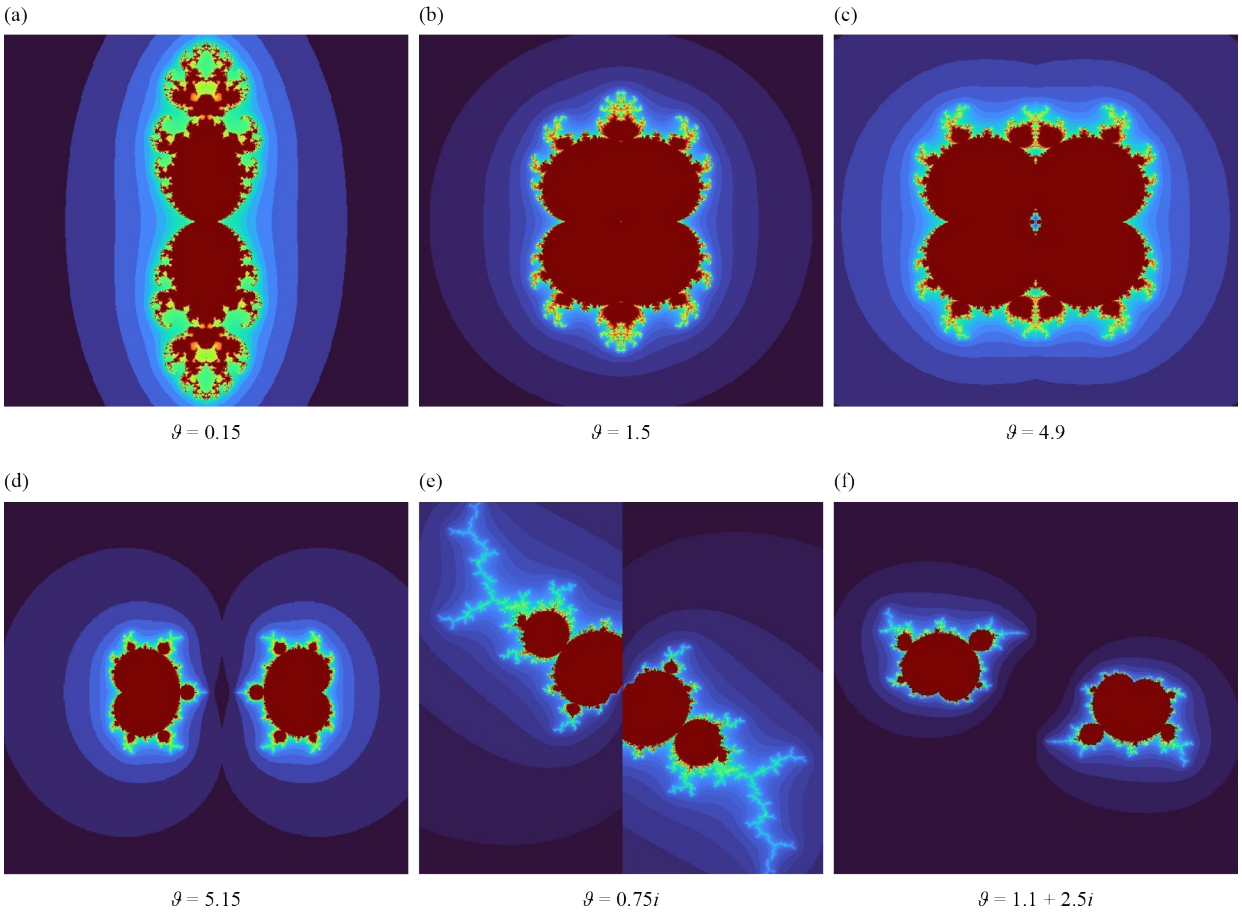


Figure 2. The effect of parameter ϑ on Mandelbrot sets generated by Algorithm 1. The execution times for the images were: (a) 1.84 s, (b) 1.98 s, (c) 2.17 s, (d) 2.54 s, (e) 2.89 s, and (f) 3.17 s

Figure 2a-f demonstrates how varying parameter ϑ significantly alters the morphology of the Mandelbrot set, while four other parameters remain fixed. Figure 2a-d show results for purely real values of ϑ, Figure 2e for purely imaginary, and Figure 2f for complex. These sets exhibit intricate, self-similar boundaries with vivid coloring: deep red central regions outlined in green, transitioning to blue tendrils and wavy purple backgrounds that indicate divergence properties. Figure 2e displays notable symmetry, while Figure 2f consists of two symmetric Mandelbrot-like sets with bulbous protrusions and concentric color layers representing escape times. Figures 3-5a-c demonstrate the significant impact

of varying parameter ψ, $\hbar$, and $\wp$, while four other parameters remain fixed. Figures 3-5a show results for purely real values, Figures 3-5b for purely imaginary, and Figures 3-5c for complex. Figure 3a-c depicts a symmetrical, three-petaled fractal structure reminiscent of a clover. Each dark red petal, representing the region of bounded iteration, is surrounded by gradients of blue and purple that indicate the speed of divergence. The intricate, green-outlined boundaries are set against a solid dark purple background, highlighting the set's complex and irregular detail across multiple scales. Figure 4a displays a striking fractal pattern with pentagonal symmetry. A central five-pointed star, colored in a gradient from dark blue to red, is encircled by five crescent-like shapes positioned at the vertices of an implied pentagon. This intricate, radially symmetric composition exhibits both mathematical structure and vivid color transitions. Figures 4b, c and 5a-c display four-petaled, cardioid-shaped fractals characteristic of Mandelbrot-like sets. The central red region denotes bounded orbits, while surrounding gradients of blue, green, and yellow encode escape times. Outer structures with smaller buds reveal self-similarity, all set against a dark purple background that accentuates the intricate boundary between stability and divergence. These patterns blend the fine detail of Rangoli art with the delicate texture of glass painting. Image generation times were recorded for each iteration.

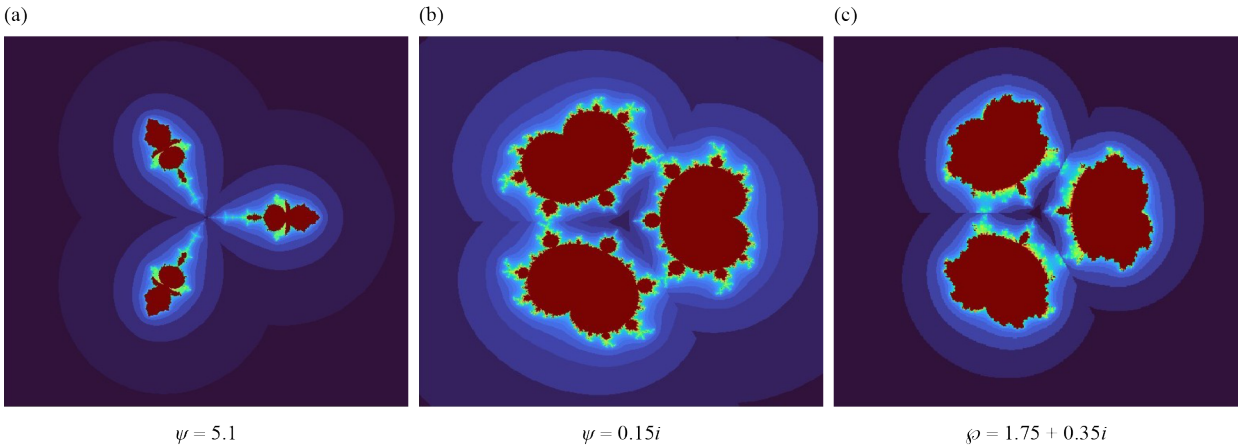


Figure 3. The effect of parameter ψ on Mandelbrot sets generated by Algorithm 1. The execution times for the images were: (a) 2.08 s, (b) 2.31 s, and (c) 2.55 s

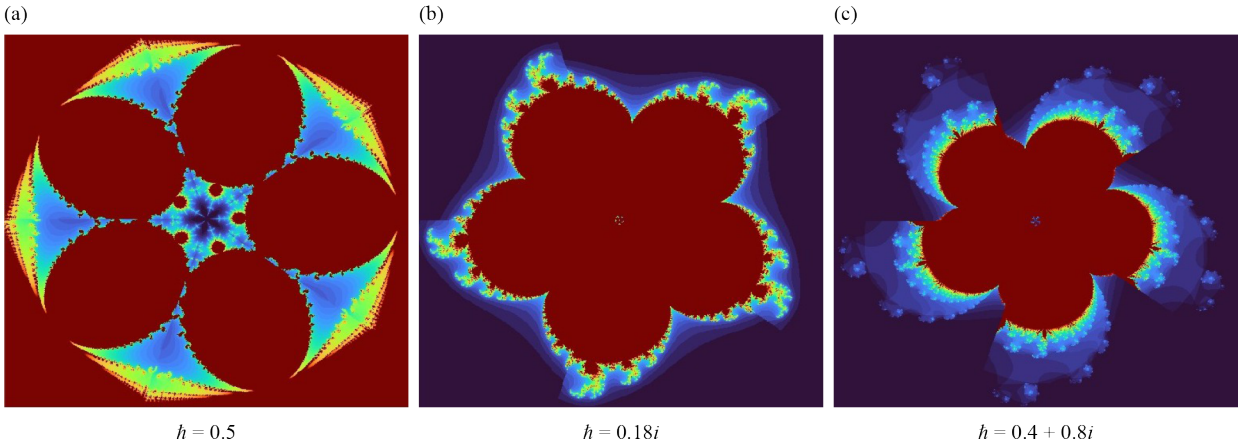


Figure 4. The effect of parameter $\hbar$ on Mandelbrot sets generated by Algorithm 1. The execution times for the images were: (a) 2.24 s, (b) 2.47 s, and (c) 2.73 s

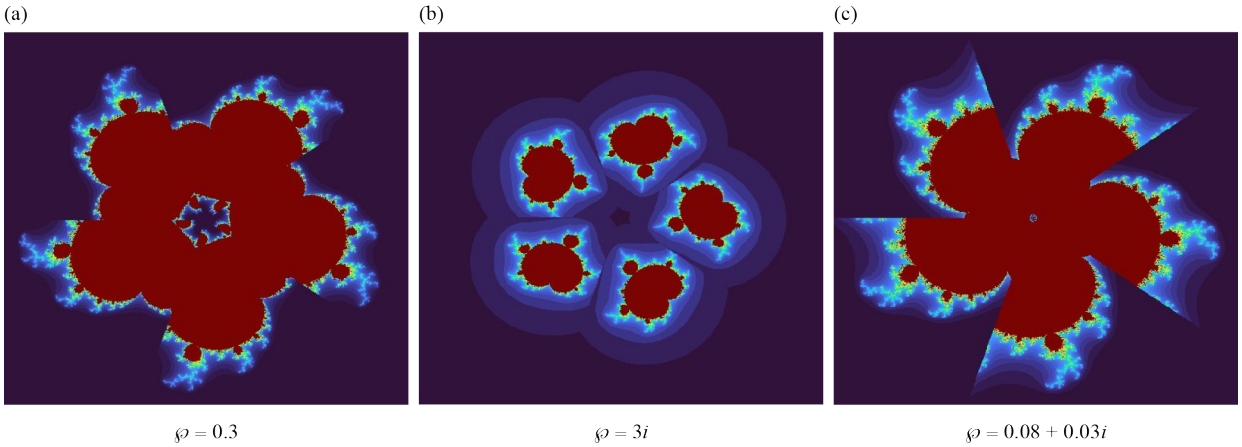


Figure 5. Mandelbrot sets generated by Algorithm 1 under varying parameter $\wp$ values, with corresponding execution times: (a) 2.44 s, (b) 2.81 s, and (c) 3.12 s

For 2nd example, Mandelbrot sets are generated by Algorithm 1 under a certain set of parameters $\phi = 0.62i$, $\hbar = 0.31i$, and $\wp = 0.06i$. The resulting images were divided into four groups to analyze the influence of specific parameters; within each group, a subset of the parameters ℓ, p, λ, and s was held constant while the remaining one was systematically varied.

(i) In Figure 6, fixed $\vartheta = -0.85$, $p = 2$, $\lambda = 0.45$, and $s = 0.75$, while ℓ varies as: (a) 3.35, (b) 6.45, (c) 26.25, (d) 12, (e) 32, (f) 64.

(ii) In Figure 7, fixed $\ell = 8$, $\vartheta = 0.85$, $p = 2$, and $s = 0.75$, while λ varies as: (a) 0.01, (b) 0.15, (c) 0.35, (d) 0.65, (e) 0.85, (f) 0.98.

(iii) In Figure 8, fixed $\ell = 6$, $\vartheta = 0.5$, $\lambda = 0.6$, and $s = 0.47$, while p varies as: (a) 2, (b) 3, (c) 4, (d) 6, (e) 11, (f) 21.

(iv) In Figure 9, fixed $\ell = 6$, $\vartheta = 0.5$, $p = 3$, and $\lambda = 0.6$, while s varies as: (a) 0.01, (b) 0.15, (c) 0.45, (d) 0.65, (e) 0.85, (f) 0.97.

Figures 6a-f contrast Mandelbrot sets generated with integer and non-integer values of ℓ. For non-integer ℓ, the fractals display complex central structures with rotational symmetry, self-similar boundaries, and filament-connected bulbs, all rendered against a dark purple background. Conversely, integer ℓ values produce ℓ identical copies arranged with perfect ℓ-fold symmetry, forming a rosette-like pattern. As ℓ increases, these copies diminish in size and begin to overlap. With further reduction in ℓ's decimal value, the overlapping intensifies and the shapes deviate from their characteristic forms, though the overall rosette-like symmetry is maintained. Figures 7a-f show that for $\ell = 8$, the Mandelbrot set consists of eight identical copies arranged in a circular, rosette-like pattern with pointed tips, resembling a star or flower-like structure. As the parameter λ increases, these individual copies grow in size and begin to overlap with one another. In Figures 8a-f, the Mandelbrot sets exhibit complex fractal geometries. Figures 8a features a structure centered on a dark purple pentagon, comprising ten irregular red blobs arranged within a wavy blue ring. Figures 8b displays six-fold rotational symmetry with rounded triangular shapes, each containing a red butterfly-like pattern and green accents, set against overlapping purple circles. The 8c-f reveal intricate symmetric arrangements, including lobed structures with 6, 11, and 21 lobes symmetrically positioned around a large central circle, all maintaining a consistent dark purple backdrop. In Figures 9a-f, the Mandelbrot sets display pronounced radial symmetry, evoking floral or star-shaped patterns. Each red lobe exhibits intricate, self-similar fractal details with finely jagged edges. The presence of a large central void and distinctly separated lobes indicates minimal structural overlap. However, as the parameter s increases, these individual copies expand in size and progressively begin to overlap. The image creation time for each iteration is also mentioned.

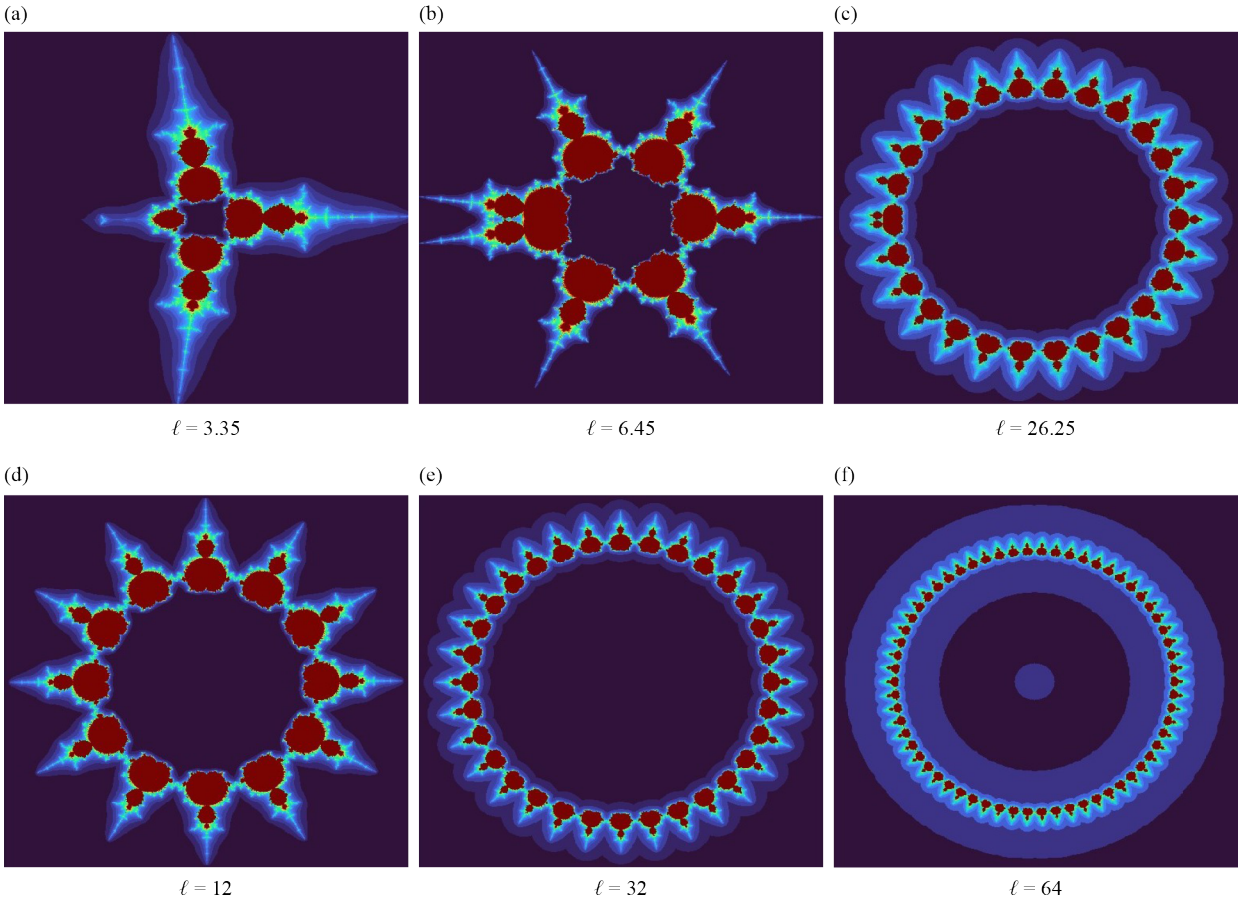
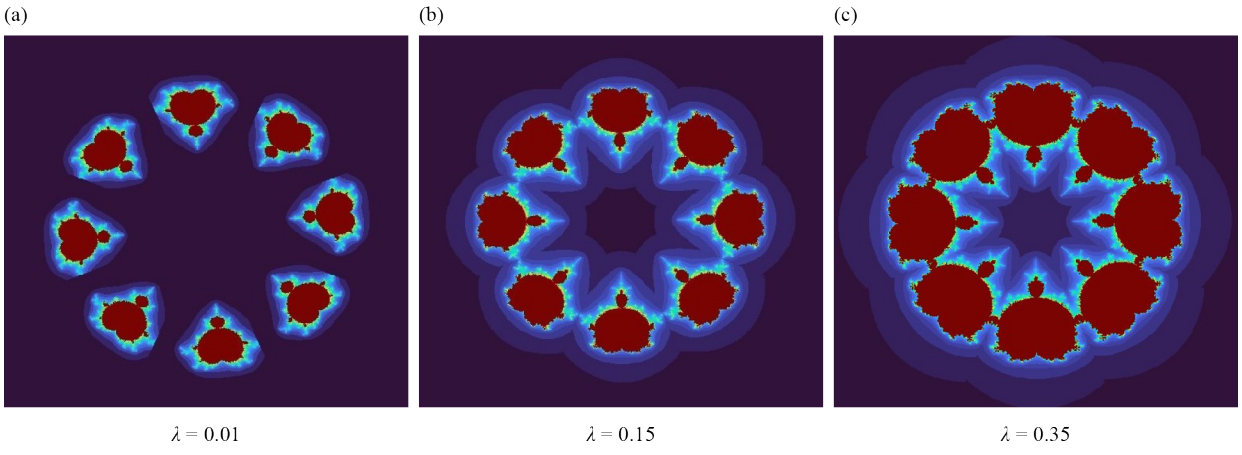


Figure 6. The effect of parameter ℓ on Mandelbrot sets generated by Algorithm 1. The execution times for the images were: (a) 1.84 s, (b) 2.05 s, (c) 2.37 s, (d) 2.84 s, (e) 3.17 s, and (f) 3.47 s



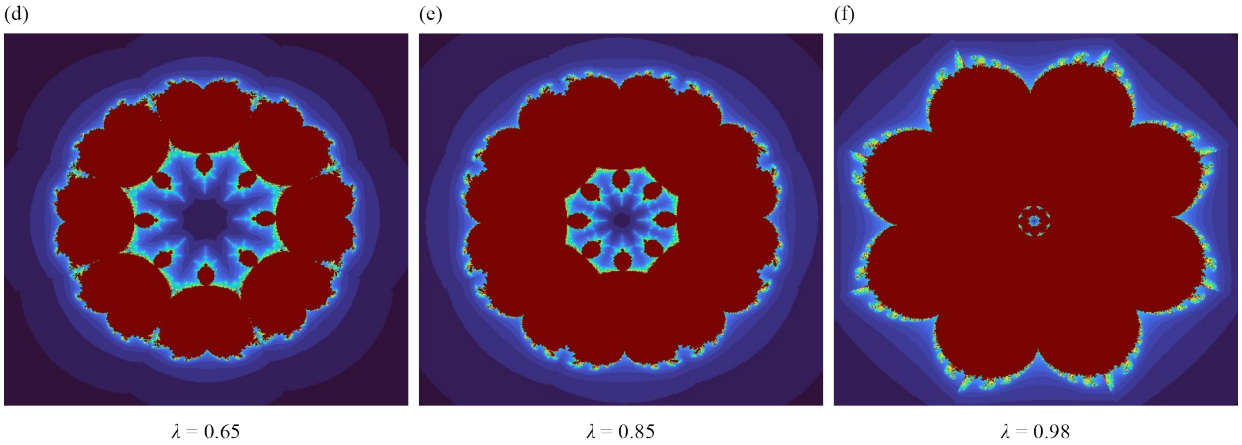


Figure 7. The effect of parameter λ on Mandelbrot sets generated by Algorithm 1. The execution times for the images were: (a) 2.14 s, (b) 2.27 s, (c) 2.57 s, (d) 2.84 s, (e) 3.05 s, and (f) 3.23 s

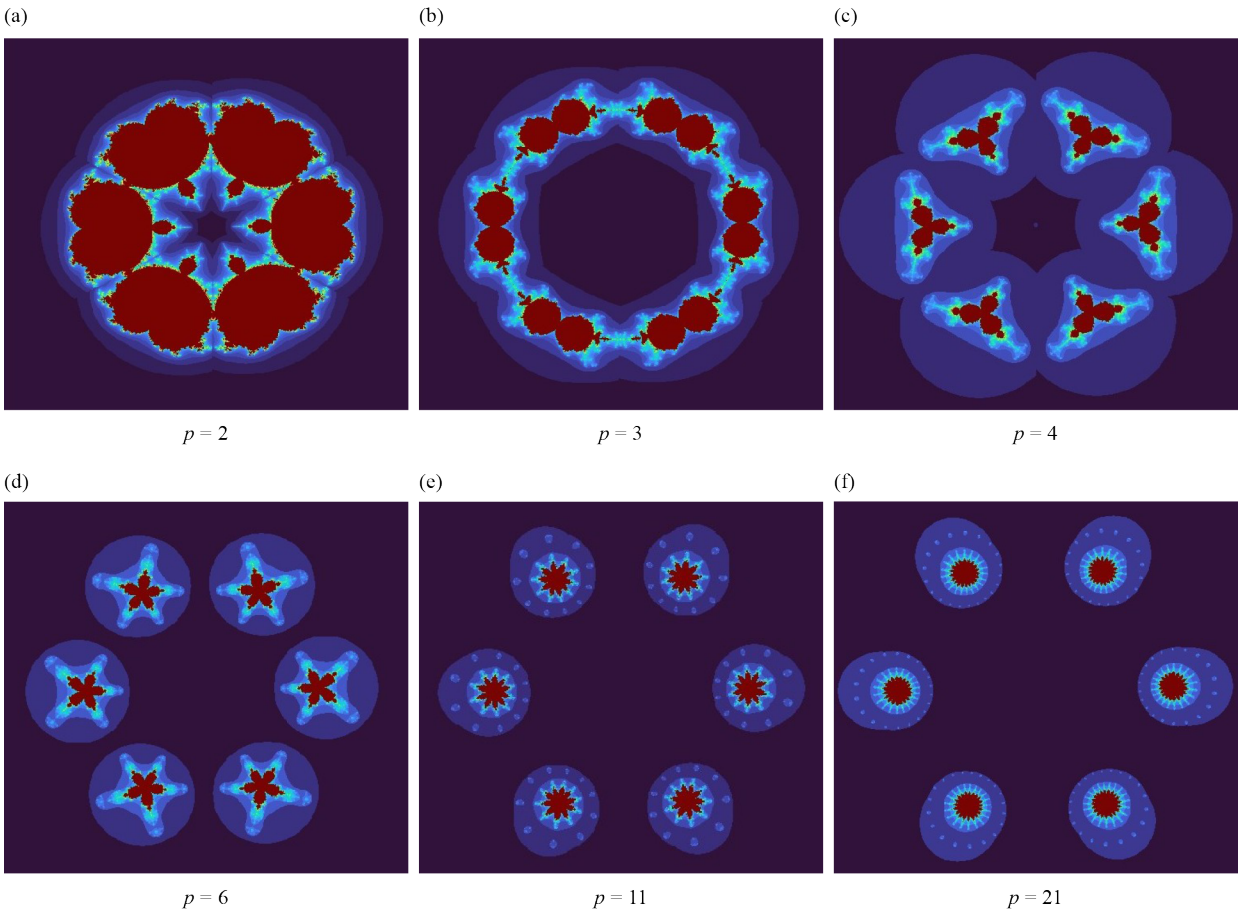


Figure 8. The effect of parameter p on Mandelbrot sets generated by Algorithm 1. The execution times for the images were: (a) 1.24 s, (b) 1.65 s, (c) 1.97 s, (d) 2.19 s, (e) 2.45 s, and (f) 2.77 s

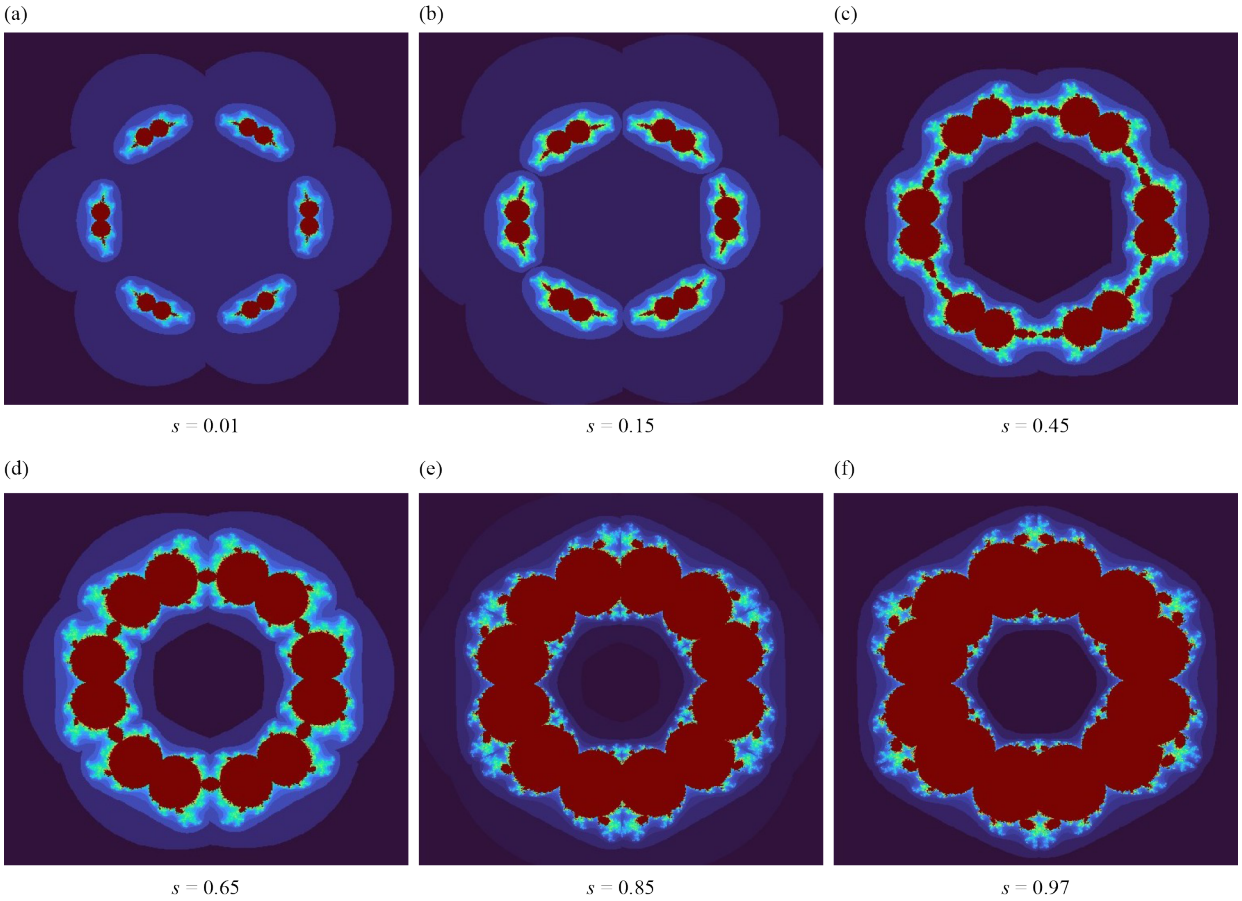


Figure 9. The effect of parameter s on Mandelbrot sets generated by Algorithm 1. The execution times for the images were: (a) 2.04 s, (b) 2.26 s, (c) 2.57 s, (d) 2.88 s, (e) 3.11 s, and (f) 3.37 s

4.2 *Mandelbrot sets for* $\Psi(z) = \vartheta\cos(z^p) + \psi z + \log(\omega^\ell)$

For the first example, we generate Mandelbrot sets by Algorithm 2 with the function $\Psi(z) = \vartheta\cos(z^p) + \psi z + \log(\omega^\ell)$. The parameters are fixed as follows: $\ell = 4$, $\lambda = 0.5$, $|\tau| = 0.6$, and $s = 0.85$. To analyze the visual effects of parameter variation, we organize the output into four groups. Within each group, three of the parameters ϑ, ψ, ω, ℓ are held constant, and the fourth is varied. The execution times for creating images are also shown in seconds.

(i) In Figure 10, fixed $\psi = 0.1$, $\hbar = 0.71$, $\wp = 0.3$, while ϑ varies as: (a) 0.4, (b) 1.4, (c) -0.4, (d) -1.2, (e) $1.15i$, (f) $0.75 + 0.5i$.

(ii) In Figure 11, fixed $\vartheta = 0.15$, $\hbar = 0.15$, $\wp = 0.5$, while ψ varies as: (a) 0.6, (b) $-0.2i$, (c) $0.15 - 0.35i$.

(iii) In Figure 12, fixed $\psi = 0.15$, $\vartheta = 0.025i$, $\wp = 0.03$, while $\hbar$ varies as: (a) 0.4, (b) $0.05i$, (c) $0.4 - 0.5i$.

(iv) In Figure 13, fixed $\psi = -0.25$, $\vartheta = 0.15i$, $\hbar = 0.5i$, while $\wp$ varies as: (a) 3, (b) $0.5i$, (c) $0.2 + 0.3i$.

Figure 10a-f demonstrates how the morphology of the Mandelbrot set transforms as the parameter ϑ varies, while four other parameters remain fixed. Figure 10a-d correspond to purely real values of ϑ, Figure 10e to purely imaginary, and 10f to complex. In Figure 10a-c, the fractal pattern exhibits symmetry across both horizontal and vertical axes, composed of repeating cardioid-like red shapes surrounded by regions of blue, green, and yellow against a dark purple background. These intricate, self-similar structures arise from iterative mathematical processes characteristic of the Mandelbrot set. Figure 10d-f display four-fold rotational and reflection symmetry across both diagonals and axes, featuring rounded red shapes at the ends of cross arms encircled by light blue areas with yellow-green speckles. Figure 10e shows pronounced symmetry, while Figure 10f consists of two symmetric Mandelbrot-like sets with bulbous protrusions and concentric

color layers indicating escape times. Figures 11-13a-c illustrate fractal patterns in the complex plane generated under different parameter conditions: Figures 11-13a uses purely real values of ψ, $\hbar$, and $\wp$; Figures 11-13b purely imaginary; and Figures 11-13c complex. The resulting structures exhibit self-similarity and intricate boundaries, characterized by a central cross-like arrangement of red shapes indicating regions of divergence in the complex function. Surrounding transitions are marked by spiky blue and green fractal edges, where iterates shift between convergence and divergence. The designs display four-fold symmetry with rounded extensions along the cardinal directions, adorned with smaller, colorful protrusions in gradients of blue, green, and yellow against a dark purple background. These patterns combine the fine detail of Rangoli art including the delicate texture of glass painting, and image generation times were tracked for iterative process.

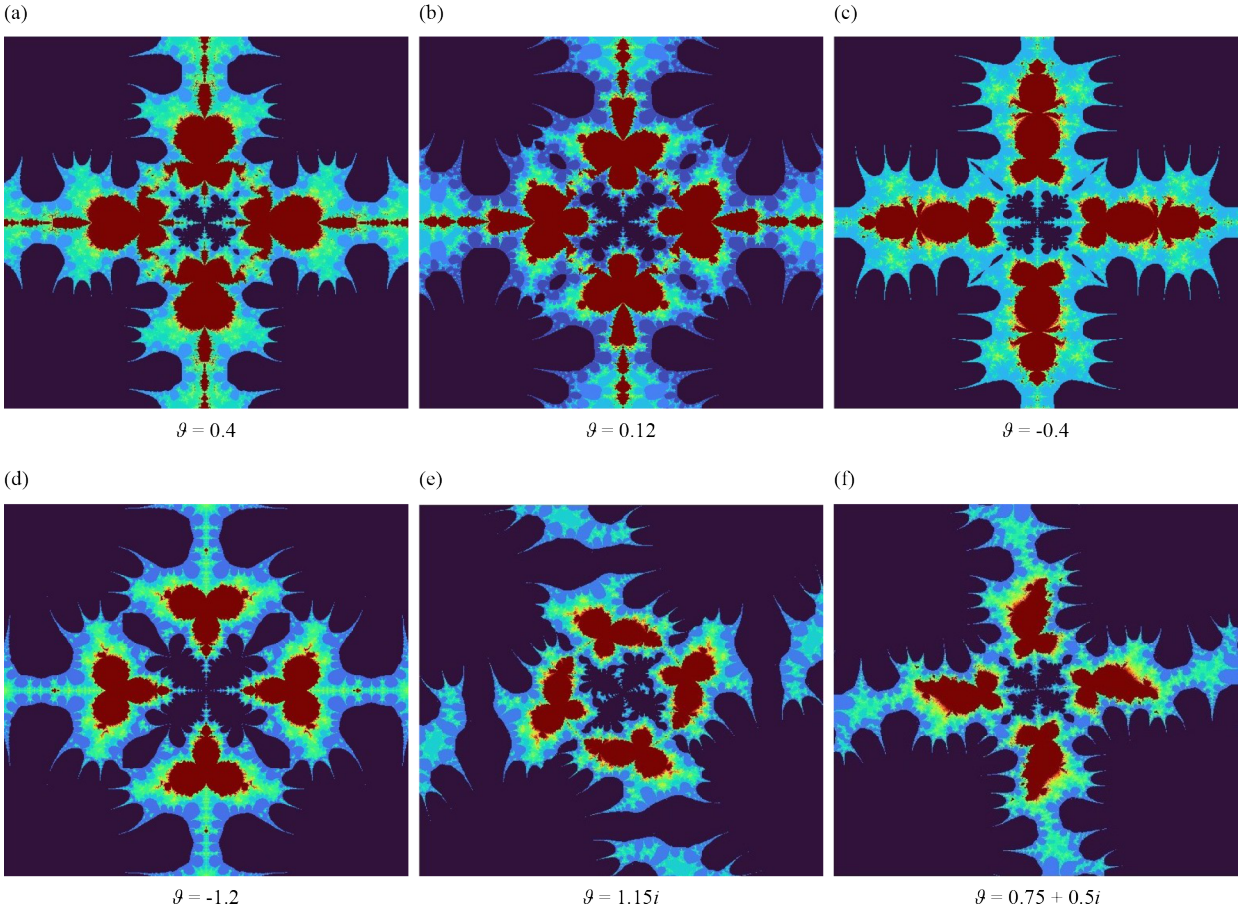


Figure 10. The effect of parameter ϑ on Mandelbrot sets generated by Algorithm 2. The execution times for the images were: (a) 0.84 s, (b) 1.05 s, (c) 1.17 s, (d) 0.84 s, (e) 1.05 s, and (f) 1.17 s

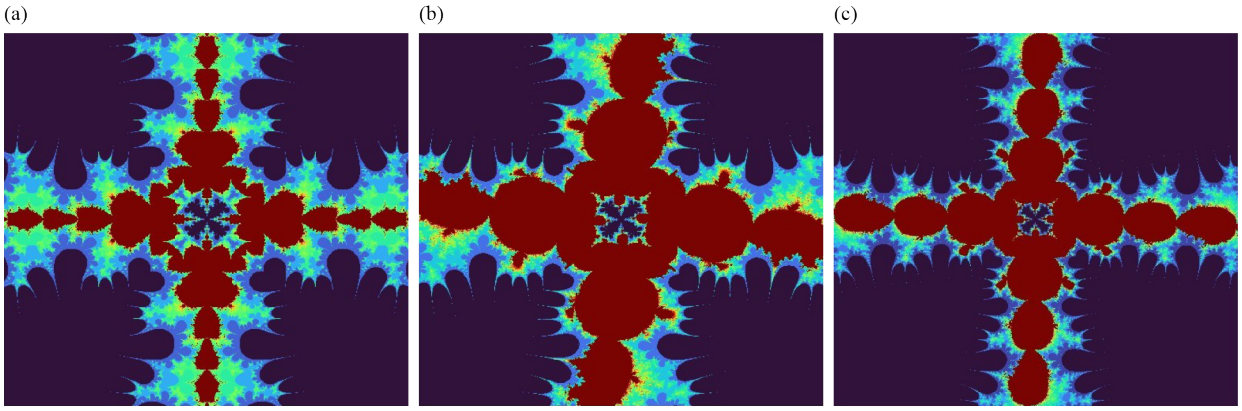


Figure 11. The effect of parameter $\wp$ on Mandelbrot sets generated by Algorithm 2. The execution times for the images were: (a) 1.08 s, (b) 1.31 s, and (c) 1.55 s

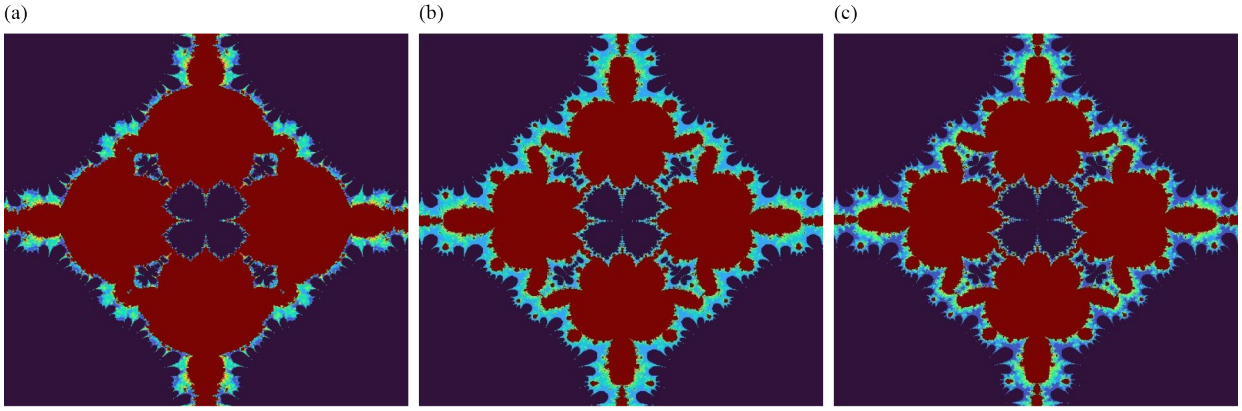


Figure 12. The effect of parameter $\hbar$ on Mandelbrot sets generated by Algorithm 2. The execution times for the images were: (a) 1.23 s, (b) 1.48 s, and (c) 1.73 s

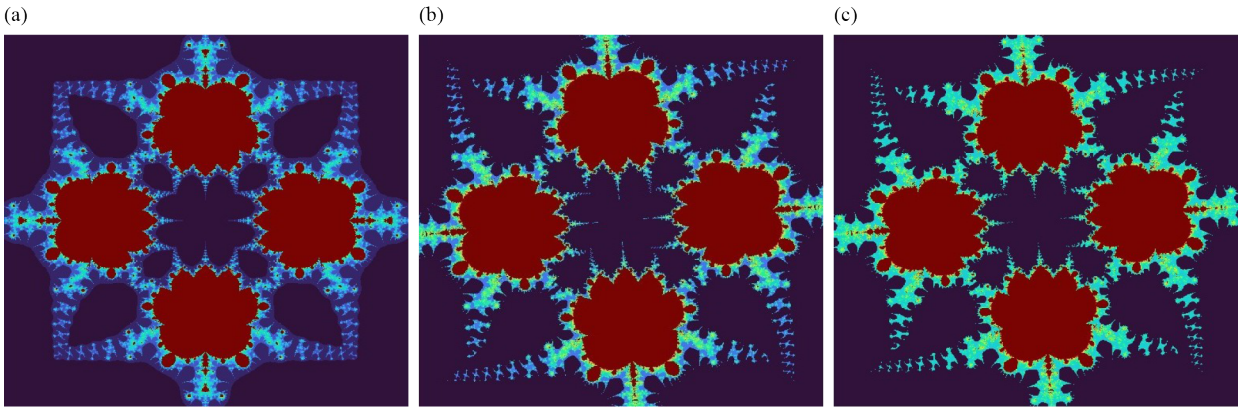


Figure 13. The effect of parameter $\wp$ on Mandelbrot sets generated by Algorithm 2. The execution times for the images were: (a) 1.64 s, (b) 1.89 s, and (c) 2.21 s

For the second example, Mandelbrot sets are generated by Algorithm 2 under a certain set of parameters $\vartheta = 1.15$, $\phi = 0.05i$, $\hbar = 0.3$, and $\wp = 0.3i$. The resulting images were divided into four groups to analyze the influence of specific parameters; within each group, a subset of the parameters ℓ, p, λ, and s was held constant while the remaining one was systematically varied.

(i) In Figure 14, fixed $p = 3$, $\lambda = 0.65$, and $s = 0.85$, while ℓ varies as: (a) 2, (b) 3, (c) 9.5, (d) 13.6, (e) 19, (f) 30.

(ii) In Figure 15, fixed $\ell = 4$, $p = 3$, and $s = 0.85$, while λ varies as: (a) 0.1, (b) 0.3, (c) 0.5, (d) 0.7, (e) 0.85, (f) 0.97.

(iii) In Figure 16, fixed $\ell = 12$, $\lambda = 0.7$, and $s = 0.65$, while p varies as: (a) 2, (b) 3, (c) 4, (d) 8, (e) 18, (f) 51.

(iv) In Figure 17, fixed $\ell = 8$, $p = 3$, and $\lambda = 0.5$, while s varies as: (a) 0.1, (b) 0.25, (c) 0.45, (d) 0.65, (e) 0.85, (f) 1.

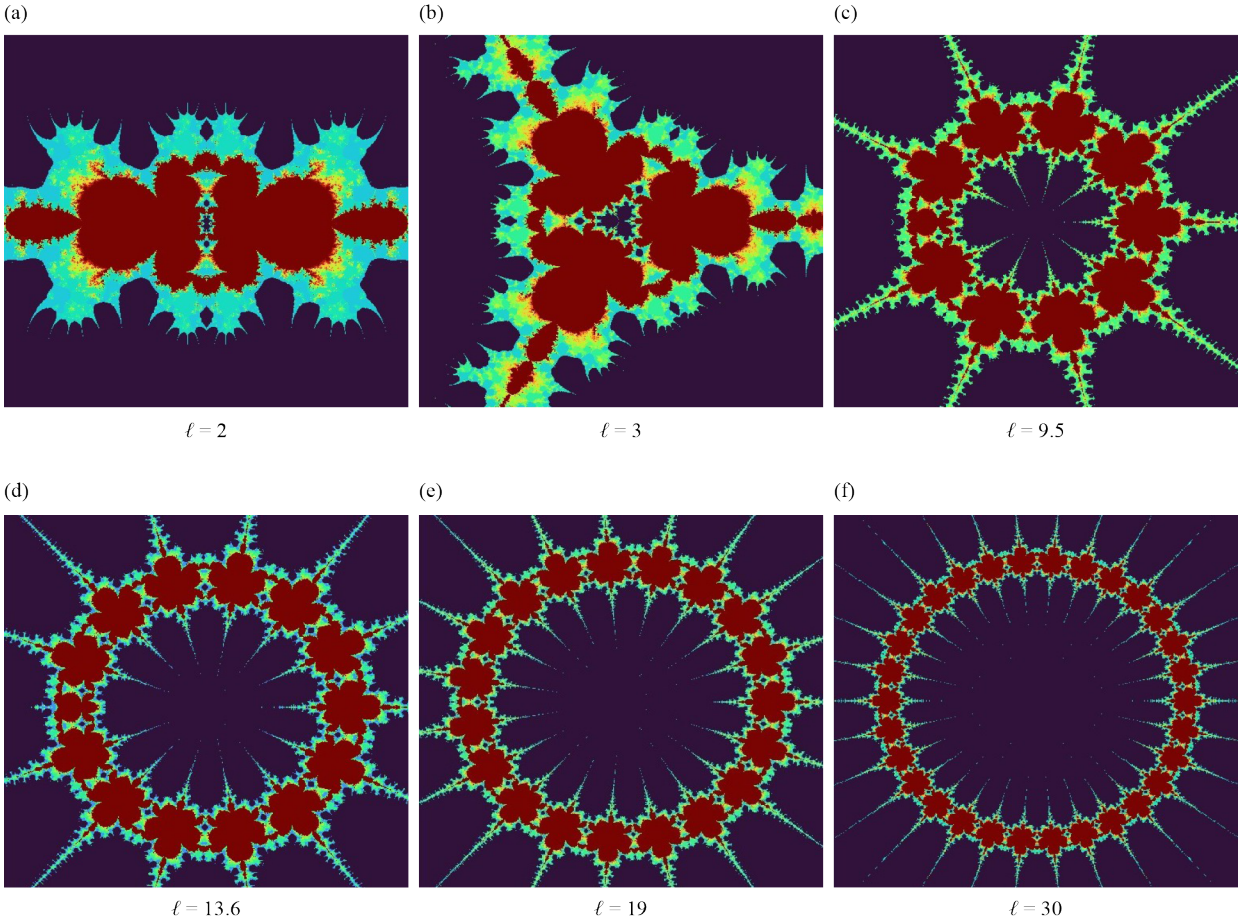


Figure 14. The effect of parameter ℓ on Mandelbrot sets generated by Algorithm 2. The execution times for the images were: (a) 1.74 s, (b) 2.05 s, (c) 2.37 s, (d) 2.84 s, (e) 3.12 s, and (f) 3.53 s

Figures 14a-f contrast Mandelbrot sets generated with integer and non-integer values of ℓ. For non-integer ℓ, the fractals exhibit complex central structures with four-fold rotational symmetry, featuring a dark red central shape that expands outward in a flower-like or star-like formation, surrounded by intricate, self-similar boundaries against a dark purple background. The symmetry is reflected across horizontal and vertical axes, with mirrored dark purple shapes at the corners and cyan backgrounds adorned with jagged yellow, orange, and red patterns. In contrast, integer values of ℓ produce ℓ identical copies arranged with perfect ℓ-fold symmetry, forming a floral or stellar pattern. As ℓ increases, these copies expand and begin to overlap. Further analysis in Figures 15-17a-f shows that as parameters p, λ, and s increase, the individual copies similarly grow in size and progressively overlap. These patterns display a central dark

purple region encircled by a neon green boundary extending into four symmetric arms, with maroon splatter-like petals at each cardinal point. The structure expands outward through repeating, scaled shapes in maroon, surrounded by green and yellow gradients transitioning to orange at the edges. The overall design exhibits four-fold rotational symmetry with scalloped edges and self-similar fractal characteristics. Figures 16c-f reveal increasingly complex symmetric arrangements, featuring lobed structures with 2, 3, 4, 8, 18, and 51 lobes positioned around a large central circle, all set against a consistent dark purple backdrop. Similarly, Figures 17a-f emphasize pronounced radial symmetry with floral or star-shaped patterns, where each red lobe displays finely jagged, self-similar details. A large central void and initially separated lobes suggest minimal overlap, though increasing parameter s causes expansion and eventual overlapping of copies. Image generation times for each iteration were recorded throughout.

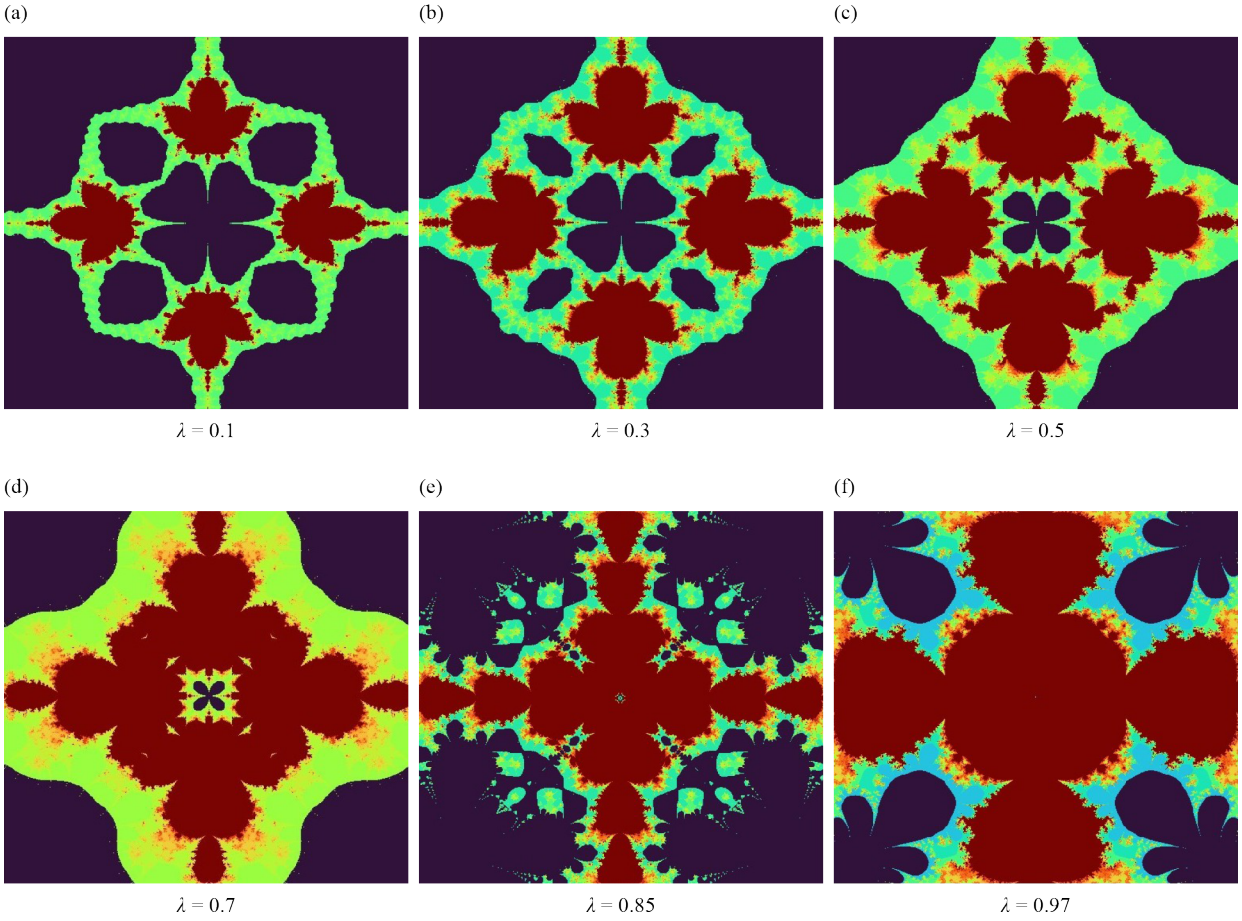


Figure 15. The effect of parameter λ on Mandelbrot sets generated by Algorithm 2. The execution times for the images were: (a) 2.84 s, (b) 3.21 s, (c) 3.54 s (d) 3.84 s, (e) 4.05 s, and (f) 4.37 s

Finally, we observe that the parameters ϑ, ψ, $\hbar$, $\wp$, ℓ, λ, p, and s profoundly affect the morphology, scale as well as intricacy of the Mandelbrot set. Depending on whether these parameters assume purely real, purely imaginary, or complex values, the resulting fractal structure is markedly transformed. In particular, increasing the values of ℓ, λ, p, and s produces increasingly elaborate patterns, evolving the central form into rosette, floral, or star-like configurations that evoke the appearance of intricate glass art or finely detailed decorative blades (Figures 2-17). It is seen that:

- The parameters ϑ, ψ, $\hbar$, $\wp$, ℓ, λ, p, and s critically determine the fractal shape, size, and colouration.
- The derived convergence criteria play a vital role in defining the resolution and pixel richness of the fractals.

• Fractals produced in this study are highly novel and visually pleasing, owing to the complex functions $\Phi(z)$ and $\Psi(z)$ used in their generation.

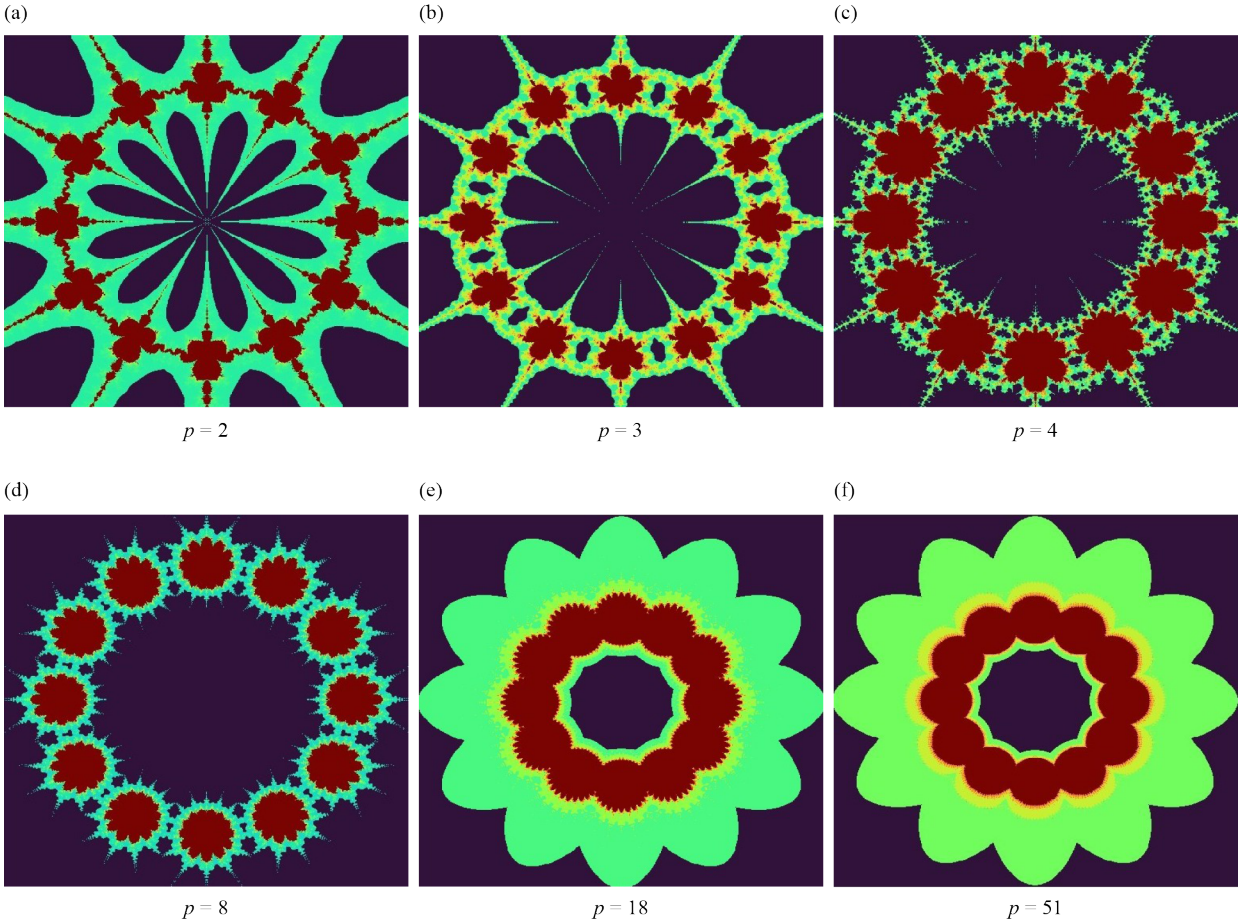
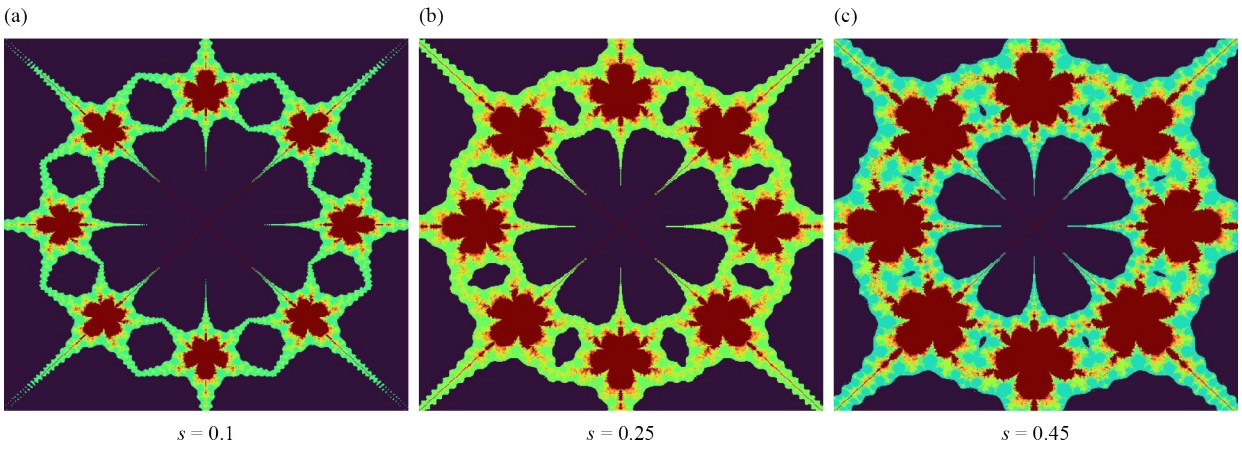


Figure 16. The effect of parameter p on Mandelbrot sets generated by Algorithm 2. The execution times for the images were: (a) 2.93 s, (b) 3.45 s, (c) 3.77 s, (d) 4.04 s, (e) 4.35 s, and (f) 4.77 s



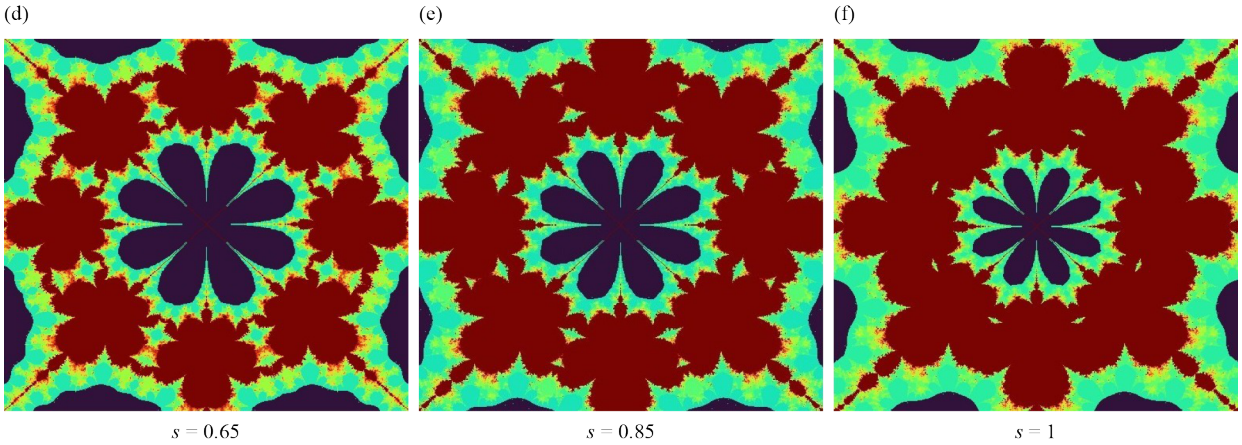


Figure 17. The effect of parameter s on Mandelbrot sets generated by Algorithm 2. The execution times for the images were: (a) 3.81 s, (b) 4.25 s, (c) 4.67 s, (d) 5.11 s, (e) 5.28 s, and (f) 5.58 s

5. Conclusion

This study established an escape criterion using the viscosity approximation iterative method with s-convexity, enabling the generation of intricate Mandelbrot sets via Algorithms 1 and 2. Implemented in MATLAB software was employed to analyze the behavior of these fractals under varying parameter values, revealing intricate and non-classical structures. Our findings show that parameters such as ψ, $\hbar$, $\wp$, ℓ, λ, p, and s significantly influence the shape, color, and complexity of the fractals—even small variations lead to noticeable changes. Future work will extend this approach to Mandelbrot sets by employing complex exponential or sine functions, and to include additional metrics such as generation time and Average Number of Iterations (ANI) in our analysis. A key objective will be the development of a standardized benchmark for fractal generation, grounded in performance metrics such as generation time and the non-escaping area index. This benchmark is crucial for enabling rigorous, quantitative comparisons and for clearly delineating the standing of algorithmic contributions within the field. Additionally, the results of this paper hold practical potential for applications in the textile industry, particularly for designing and printing purposes.

Acknowledgments

The authors gratefully acknowledge Qassim University, represented by the Deanship of Graduate Studies and Scientific Research, on the financial support for this research under the number (QU-J-UG-2-2025-56963) during the academic year 1446 AH/2024 AD.

Conflict of interest

The authors declare no competing financial interest.

References

[1] Julia G. Mémoire sur l'iteration des fonctions rationnelles [Dissertation on the iteration of rational functions]. *Journal of Pure and Applied Mathematics*. 1918; 8: 47-245.

[2] Mandelbrot BB. *The Fractal Geometry of Nature*. San Francisco: Freeman; 1982.

[3] Jolaoso L, Khan S, Aremu K. Dynamics of RK iteration and basic family of iterations for polynomiography. *Mathematics*. 2022; 10(18): 3324. Available from: https://doi.org/10.3390/math10183324.

[4] Gdawiec K, Kotarski W, Lisowska A. On the robust Newton's method with the Mann iteration and the artistic patterns from its dynamics. *Nonlinear Dynamics*. 2021; 104(1): 297-331. Available from: https://doi.org/10.1007/s11071-021-06306-5.

[5] Muthukumar P, Balasubramaniam P. Feedback synchronization of the fractional order reverse butterfly-shaped chaotic system and its application to digital cryptography. *Nonlinear Dynamics*. 2013; 74: 1169-1181. Available from: https://doi.org/10.1007/s11071-013-1032-3.

[6] Nakamura K. Iterated inversion system: an algorithm for efficiently visualizing Kleinian groups and extending the possibilities of fractal art. *Journal of Mathematics and the Arts*. 2021; 15: 106-136. Available from: https://doi.org/10.1080/17513472.2021.1943998.

[7] Kang SM, Rafiq A, Latif A, Shahid AA, Kwun YC. Tricorns and multicorns of *s*-iteration scheme. *Journal of Function Spaces*. 2015; 2015: 417167. Available from: https://doi.org/10.1155/2015/417167.

[8] Kumari S, Gdawiec K, Nandal A, Kumar N, Chugh R. Fractal generation in modified Jungck-S orbit. *IEEE Access*. 2019; 235: 35060-35071. Available from: https://doi.org/10.1109/ACCESS.2019.2904677.

[9] Phuengrattana W, Suantai S. On the rate of convergence of Mann, Ishikawa, Noor and SP-iterations for continuous functions on an arbitrary interval. *Journal of Computational and Applied Mathematics*. 2011; 235(9): 3006-3014. Available from: https://doi.org/10.1016/j.cam.2010.12.022.

[10] Usurelu GI, Bejenaru A, Postolache M. Newton-like methods and polynomiographic visualization of modified Thakur processes. *International Journal of Computer Mathematics*. 2021; 98: 1049-1068. Available from: https://doi.org/10.1080/00207160.2020.1802017.

[11] Fatou P. Sur les équations fonctionnelles [On functional equations]. *Bulletin of the French Mathematical Society*. 1919; 47: 161-271.

[12] Ahmad I, Sajid M, Ahmad R. Julia sets of transcendental functions via a viscosity approximation-type iterative method with *s*-convexity. *Statistics, Optimization and Information Computing*. 2024; 12: 1553-1572. Available from: https://doi.org/10.19139/soic-2310-5070-1918.

[13] Kwun YC, Tanveer M, Nazeer W, Gdawiec K, Kang SM. Mandelbrot and Julia sets via Jungck-CR iteration with *s*-convexity. *IEEE Access*. 2019; 7: 12167-12176. Available from: https://doi.org/10.1109/ACCESS.2019.2892013.

[14] Zhang HX, Tanveer M, Li YX, Peng QX, Shah NA. Fixed point results of an implicit iterative scheme for fractal generations. *AIMS Mathematics*. 2021; 6: 13170-13186. Available from: https://doi.org/10.3934/math.2021761.

[15] Adhikari N, Sintunavarat W. The Julia and Mandelbrot sets for the function $z^p - qz^2 + rz + \sin c^w$ exhibit Mann and Picard-Mann orbits along with *s*-convexity. *Chaos, Solitons and Fractals*. 2024; 18: 114600. Available from: https://doi.org/10.1016/j.chaos.2024.114600.

[16] Tanveer M, Nazeer W, Gdawiec K. On the Mandelbrot set of $z^p + \log c^t$ via the Mann and Picard-Mann iterations. *Mathematics and Computers in Simulation*. 2023; 209: 184-204. Available from: https://doi.org/10.1016/j.matcom.2023.02.012.

[17] Maudafi A. Viscosity approximation methods for fixed-points problems. *Journal of Mathematical Analysis and Applications*. 2000; 241(1): 46-55.

[18] Kumari S, Gdawiec K, Nandal A, Postolache M, Chugh R. A novel approach to generate Mandelbrot sets, Julia sets and biomorphs via viscosity approximation method. *Chaos, Solitons and Fractals*. 2022; 163: 112-140. Available from: https://doi.org/10.1016/j.chaos.2022.112540.

[19] Husain A, Nanda MN, Chowdary MS, Sajid M. Fractals: an eclectic survey, Part-I. *Fractal and Fractional*. 2022; 6(2): 89. Available from: https://doi.org/10.3390/fractalfract6020089.

[20] Husain A, Nanda MN, Chowdary MS, Sajid M. Fractals: an eclectic survey, Part-II. *Fractal and Fractional*. 2022; 6(7): 379. Available from: https://doi.org/10.3390/fractalfract6070397.

[21] Pinheiro M. *s*-convexity, foundations for analysis. *Differential Geometry and Dynamical Systems*. 2008; 10: 257-262.